Springer

KSME

Journal of Mechanical Science and Technology 24 (3) (2010) 657~669
www.springerlink.com/content/1738-494x
DOI 10.1007/s12206-010-0112-2

Plastic continuum models for truss lattice materials with cubic symmetry †

Taehyo Park[1], Won-Sup Hwang[2] and Jong Wan Hu[1,*]

[1]*Department of Civil and Environmental Engineering, Hanyang University, Seoul, 133-791, Korea*
[2]*Department of Civil and Environmental Engineering, Inha University, Incheon, 402-751, Korea*

(Manuscript Received December 26, 2008; Revised September 8, 2009; Accepted December 16, 2009)

Abstract

Analytical and numerical studies on continuum models for the elastic-plastic behavior of uniformly periodic lattice materials under multi-axial loading are presented in this paper. This study firstly investigates the basic topology of unit cell structures for three different lattice materials with cubic symmetry. By homogenizing the mechanical properties of these materials within the unit volume space, the equivalent continuum models are obtained with the internal variables which result in the mechanical and geometrical characteristics of discrete truss members at the micro-scale such as structural packing, axial stiffness, and material density. Therefore, in this study, the strain hardening was applied to the material model of individual truss members in a valuable effort to explain the plastic behavior of the homogenized lattice material. The expansion of pressure-dependent stress surface at the macro-scale level is estimated by analytical predictions, which are derived from the equivalent continuum models. Analytical predictions show good agreements with existing results obtained by finite element (FE) analyses.

Keywords: Homogenization; Cubic symmetry; Unit cell element; Constitutive model; Stress surface

1. Introduction

Truss-lattice structures with low relative density are manufactured from high strength alloys through a simple high press forming process. These structures are fabricated by packing bent nodes with an interwoven polynomial punched layer [1]. It is assumed that the robust welding is applied to nodal connections. Lattice materials are widely used as the cores of sandwich plates since they present the opportunity to add superior stiffness-to-weight effect to the sandwich plates [2, 3]. In addition, they have been used in multifunctional applications ranging from ultra lightweight materials to automotive and aerospace components, construction materials, furniture, and sporting tools, for all of which both lower fabrication cost and higher ultimate strength are essential requirements [4, 5].

The lattice materials are composed of a characteristic unit cell element that is in a uniform periodic replication. For this reason, this smallest unit cell element is taken as the representative volume element (RVE) which represents the mechanical performance and properties of the bulk lattice material. There have been a number of investigations into this relatively new material including effective elastic properties, multi-functionality and multi-stress failure surface of unit cell structures [6-9]. The unit cell structures with the higher order of symmetry such as the cubic symmetry are considered in this study.

Cubic-symmetric unit cells take advantage of the stable packing of successive layers by sharing identical volume fractions with surrounding truss members. This packing system enables lattice materials to maximize the stiffness effect and lightweight effect within the limited volume space [10].

Deshpande et al. [2] investigated the effective properties of the unit cell of octet-truss materials. They assumed that struts are pin-jointed at all nodes so that the contribution from bending resistance to the total stiffness is negligible when compared to that from stretching of the struts. They reported combined analytical and finite element (FE) investigations of the perfectly elasto-plastic failures as well as collapse modes owing to elastic buckling. The predictions were compared with experimental observations from the test on an octet-truss. These periodic lattice materials, which are stretching dominated, have been developed to supply high axial stiffness and strength as well as multi-functional weight efficient for their practical applications.

Recent researches developed a general homogenization procedure for practical lattice structures [2, 11-13]. They have been involved with the continuum modeling of repetitive lattice structures including micro-macro stress-strain relationship regarding force and displacement, discrete-filed method, small-strain homogenization technique, and energy equivalent

† This paper was recommended for publication in revised form by Associate Editor Tae Hee Lee

*Corresponding author. Tel.: +1 404 625 3501, Fax.: +1 404 894 2278
E-mail address: jongwan.hu@ce.gatech.edu

concept. The lattice material was viewed as a composite material with elastic-plastic truss members embedded in an infinite soft matrix. Based on this assumption, the general finite-strain plasticity model was developed.

In this study, the macroscopic continuum constitutive models are developed for predicting the mechanical behavior of the unit cell structures subjected to multi-axial loading in the plastic regime. The relative density, a key parameter in determining the effective strength of the unit cell structure, is evaluated from the volume fractions of individual truss members. The elastic moduli under uni-axial states are investigated within a reasonable range of the relative density. On the basis of constitutive equations obtained, the macro-scale stress surface is analytically determined by examining whether the stress state in micro-scale lattice truss members reaches the limit state of the micro-scale stress under multi-axial loading. The accuracy of these predicted stress surfaces is verified with the numerical experimental results obtained from finite element (FE) analyses.

2. Topological characteristics of unit cell structures

The lattice materials are constructed by stacking unit cell elements face to face in perfect alignment in three dimensions. By repeating the prototype unit along the material's principal axes, a regular structure of the lattice material can be obtained. The unit cell element is the unit component that still possesses all physical characteristics of the bulk lattice material [14, 15]. Therefore, one can consider a single unit cell in the numerical simulation as the representative element of the entire lattice material, assuming that the lattice material is infinitely matrix material [11, 12].

To achieve the convenience of analysis, we introduce sub-lattice elements. Sub-lattice elements are defined as the least sub-structure that composes the unit cell element and that represents the basic material property of the symmetry base-lattice structure with only three truss members. The topological geometries of sub-lattice elements and the longitudinal axes of truss members are shown in Fig. 1. They are classified as a cubic-lattice element (Fig. 1(a)), octet-lattice element (Fig. 1(b)), and diagonal-lattice element (Fig. 1(c)) in this study. Three truss members have the length either L or $\sqrt{2}$L, the same rotational angle (θ) and nodal connectivity within the unit volume ($V_{unit} = L^3$). Therefore, strength and stiffness of its own truss member is uniform along the global axis.

All component truss members are transformed from their local axis to the global (X, Y, Z) coordinate system with the unit vector $\mathbf{a}^{(k)}$ summarized in Table 1. The superscript k indicates a truss member number. The global axes are replaced with a single subscript i=1, 2, and 3 in the vector notation such that X↔1, Y↔2, and Z↔3. The unit direction vector $\mathbf{e} = \{e_1 \quad e_2 \quad e_3\}$ should be used to separate the common vector component $\alpha^{(k)}$ as a scalar value from the unit vector $\mathbf{a}^{(k)}$ that the axis of the k^{th} truss member is making with the local coordinate axes. This unit vector $\mathbf{a}^{(k)}$ can be obtained from $\mathbf{a}^{(k)} = \alpha^{(k)} \cdot \mathbf{e}$, so the unit vector possesses three components $\mathbf{a}^{(k)} = \{\alpha_1^{(k)} \quad \alpha_2^{(k)} \quad \alpha_3^{(k)}\}$. The common vector components for the cubic-lattice element, octet-lattice element, and diagonal-lattice element are denoted by $\alpha^{(cub)}$, $\alpha^{(oct)}$, and $\alpha^{(dia)}$, respectively. They are taken as the value of $\alpha^{(cub)} = 1.0$, $\alpha^{(oct)} = \sqrt{2}/2$, and $\alpha^{(dia)} = \sqrt{2}/2$. These common vector components are determined by the absolute value of the direct cosine between the longitudinal axis of each truss member and its closest-angled global coordinate axis ($\alpha = |\cos\theta|$).

All truss members in the cubic-lattice element (Fig. 1(a)) are placed at (L,0,0), (0,L,0), and (0,0,L) position with $\alpha^{(cub)} = 1.0$. As a result, this topological system takes advantage of the strong axial stiffness along the global coordinate axes X, Y, and Z. This cubic-lattice element is utilized to strengthen uni-directional stiffness. The longitudinal direction of octet-truss members (↖, (0,L,0)→ (L,0,0)) is normal to that of diagonal-truss members (↗, (0,0,0)→ (0,L,L)) at the same surface plane of the unit volume. However, the stiffness distributions due to axial responses along the global axes remain the same in octet-lattice elements and diagonal-lattice elements. These sub-lattice elements are stacked as the cubic symmetry base element, which results in the unit cell element (e.g. octet unit cell element). In other words, the unit cell element is easily fabricated by periodically replicating these sub-lattice elements with rotational mirror symmetry.

In this study, three typical lattice materials with the cubic-

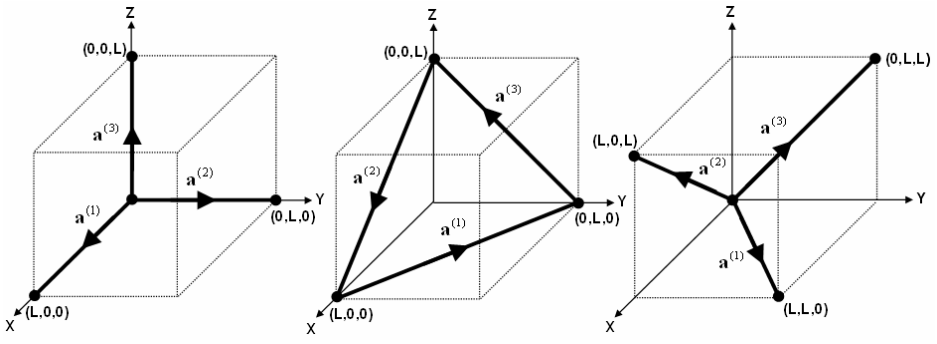

(a) Cubic-lattice element (b) Octet-lattice element (c) Diagonal-lattice element

Fig. 1. Basic topolies of sub-lattice elements.

Table 1. Unit vectors and common vector components of truss elements within sub-lattice elements.

Sub-Lattice Element	Unit Vector	e_1	e_2	e_3
Cubic-Lattice Element	$\mathbf{a}^{(1)}$	$\alpha^{(cub)}$	0	0
	$\mathbf{a}^{(2)}$	0	$\alpha^{(cub)}$	0
	$\mathbf{a}^{(3)}$	0	0	$\alpha^{(cub)}$
Octet-Lattice Element	$\mathbf{a}^{(1)}$	$-\alpha^{(oct)}$	$\alpha^{(oct)}$	0
	$\mathbf{a}^{(2)}$	$\alpha^{(oct)}$	0	$-\alpha^{(oct)}$
	$\mathbf{a}^{(3)}$	0	$\alpha^{(oct)}$	$-\alpha^{(oct)}$
Diagonal-Lattice Element	$\mathbf{a}^{(1)}$	$\alpha^{(dia)}$	$\alpha^{(dia)}$	0
	$\mathbf{a}^{(2)}$	0	$\alpha^{(dia)}$	$\alpha^{(dia)}$
	$\mathbf{a}^{(3)}$	$\alpha^{(dia)}$	0	$\alpha^{(dia)}$

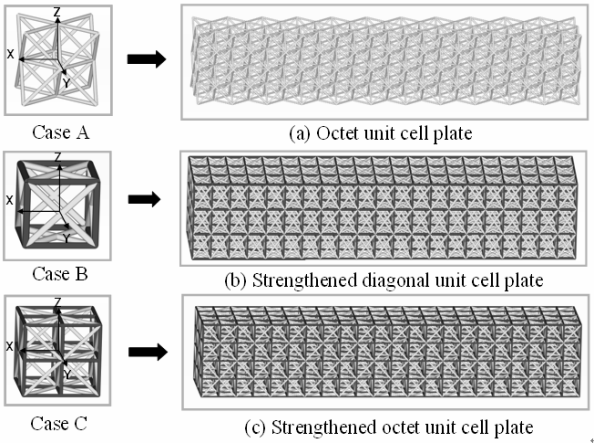

Fig. 2. Unit cell elements and their packing.

symmetric unit cell elements are addressed. Their unit cell elements, global coordinates, and structural packing are presented in Fig. 2. Three unit cell elements such as the octet unit cell (Case A), strengthened diagonal unit cell (Case B), and strengthened octet unit cell (Case C) defined herein are selected to investigate the mechanical behavior of the unit cell and the lattice material because these are the structures that are most often used in practice.

Truss members, which are solid struts in the unit cell, have their mirror symmetric pair labelled "SE1" and "SE2" in Fig. 3 (a). In fact, this symmetry in the lower scale results from the bulk lattice material in the higher symmetry. This geometric symmetry reduces 81 independent elastic constants (i.e.C_{ijkl}; I, j, k, l=1⋯3) in the constitutive matrix to 3 (i.e. C_{1111}, C_{1122}, and C_{1212}). As shown in Fig. 3(b), the octet unit cell (Case A) consists of eight tetrahedrons. Each tetrahedron component is replicated and packed with mirror planes or 90 degree rotations at each axis (see Fig. 3(a)). All truss members on the mirror planes are equally distributed into their neighboured unit volume elements. They are also aligned with the same rotational angle on the mirror plane. Therefore, the mechanical

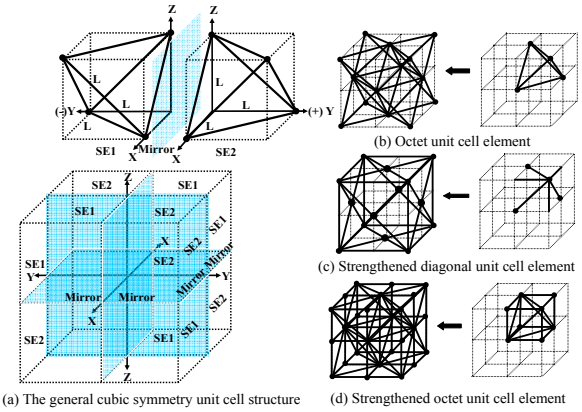

Fig. 3. Typical unit cell structures with the cubic symmetry.

properties of component truss members with respect to compliance, stiffness, and volume fraction have a significant influence on the effective material model in the octet unit cell element (see Fig. 3(b)). On the other hand, other two unit cell elements, Case B (Fig. 3(c)) and Case C (Fig. 3(d)), are strengthened by cubic-lattice elements, which possess truss members parallel to the principal axes. Owing to cubic-lattice elements, these two unit cell elements can produce the distinct uni-axial strength at the constitutive model.

All truss members have the same cross section area ($A_o = \pi r^2$) and the ratio of the radius of the truss member to the length of cubic unit volume space (r/L) is identical in all three cases. The relative density of the unit cell element ρ^*, which is defined as the ratio of the density of the lattice material to the density of the solid material in the same amount of unit volume (i.e. $\rho^* = \rho/\rho_s$), can be also expressed in terms of the ratio r/L. The relative density of a unit cell element is used to represent a metric level for significant characterization of the mechanical properties of the lattice material. It was typically taken as the value of 0.1 ($r/L = 0.1$) for generating structures with reasonable relative density [2, 8].

3. Macroscopic models

3.1 Volumetric homogenization

To calculate the overall properties of a heterogeneous material, the representative volume elements (RVE s) are used in the analysis. RVE is defined as a continuum element, which is a statistical ensemble of micro-scale objects surrounded by the continuous macro-scale media. RVE should contain the sufficiently large number of micro-scale objects in order to represent a statistical sample of the continuum mechanical properties. In the periodic medium, RVE corresponds to the unit cell element. Two different scales exist: the structure is heterogeneous at the micro-scale level, while it is viewed homogeneous at the macro-scale level [16].

The average stress $\mathbf{\Sigma}$ for the RVE defined in the global coordinates system $\mathbf{X}$ is obtained by averaging the local stress $\boldsymbol{\sigma}$ in the local coordinate system $\mathbf{x}$ over the volume of the RVE [16],

$$\mathbf{\Sigma}[\mathbf{X}] = \frac{1}{\mathrm{V}}\int_{\mathrm{V}} \boldsymbol{\sigma}[\mathbf{x}]\mathbf{A}[\mathbf{x};\mathbf{X}]d\mathrm{V}[\mathbf{x}] \tag{1}$$

where **A** denotes the linear transformation operator from the local to global coordinates. When the local medium in the RVE is discrete (as truss members), the volume-averaging operation is simplified greatly. Note that this averaging operation is valid for any type of lattice structure regardless of its symmetry property [10].

The homogenization theory is applied to describe the relationship between micro-scale and macro-scale levels of the truss-lattice material. Every discrete solid truss member, defined as the micro-scale medium in the unit cell element, has its own arbitrary orientation. To formulate the macro-scale continuum property, it is necessary to transform every individual local orientation into the global coordinate system that is a reference coordinate system in the homogenization procedure. The procedure of the homogenization is separated into the transformation ($\sigma_{11} = \sigma^{(1)}\alpha_1^{(1)} \cdot \alpha_1^{(1)}$) and average ($\Sigma_{11} = (\mathrm{V}^{(1)}/\mathrm{V}_{\mathrm{unit}})\sigma_{11}$) as shown in Fig. 4. The homogenization for one truss member under uni-axial loading in the lattice material is illustrated in this figure. In the unit volume space, the macro-scale uni-axial strain E_{11} is defined as the applied uni-axial displacement Δ_{11} divided by the length L ($\mathrm{E}_{11} = \Delta_{11}/\mathrm{L}$) of the unit volume. When homogenized, the strength of every truss member is uniformly distributed in the unit volume space as a result of the volume average of the stress of local truss members [7].

3.2 Effective constitutive models

Suppose the RVE consists of *K* discrete truss members and only the axial stress is formed uniformly in the whole length of the members. Then, the average stress is

$$\begin{aligned}\Sigma_{\mathrm{ij}} &= \frac{1}{\mathrm{V}}\sum_{k=1}^{K}\sigma^{(k)}\mathrm{A}_{\mathrm{ij}}^{(k)}(A_{(k)}\mathrm{L}_{(k)}) \\ &= \sum_{k=1}^{K} v_{\mathrm{v}}^{(k)}\sigma^{(k)}\mathrm{A}_{\mathrm{ij}}^{(k)}\end{aligned} \tag{2}$$

where $\sigma^{(k)}$, $\mathrm{L}_{(k)}$ and $A_{(k)}$ are the axial stress and the length and cross section area of the k^{th} truss. Here, the volume fraction of the k^{th} truss member is $v_{\mathrm{v}}^{(k)} = (A_k\mathrm{L}_k)/\mathrm{V}_{\mathrm{unit}}$ and $\mathrm{V}_{\mathrm{unit}}$ is the volume of the unit cell. In this case, it can be shown that the linear transformation operator A_{ij} is reduced to the product of the vector components $\mathrm{a}_{\mathrm{i}}^{(k)}$ such as $\mathrm{A}_{\mathrm{ij}}^{(k)} = \mathrm{a}_{\mathrm{i}}^{(k)} \cdot \mathrm{a}_{\mathrm{j}}^{(k)}$.

The general macro-scale strain is defined as the applied displacement load divided by the length of the square unit cell (L)

$$\mathrm{E}_{\mathrm{ij}} = \frac{\Delta_{\mathrm{ij}}}{\mathrm{L}} \tag{3}$$

Now, the macro-scale strain in the global coordinates (E_{ij}) and the local strain in the k^{th} truss member ($\varepsilon^{(k)}$) are related by

$$\varepsilon^{(k)} = \mathrm{A}_{\mathrm{ij}}^{(k)}\mathrm{E}_{\mathrm{ij}} \tag{4}$$

or

$$\mathrm{E}_{\mathrm{ij}} = \mathrm{A}_{\mathrm{ij}}^{(k)-1}\varepsilon^{(k)} . \tag{5}$$

In Eq. (5), the property that $\mathrm{A}_{\mathrm{ij}}^{(k)\text{-}1}$ also results in a symmetric unitary second order tensor (so that $\mathrm{A}_{\mathrm{ij}}^{(k)-1} = \mathrm{a}_{\mathrm{i}}^{(k)-1} \cdot \mathrm{a}_{\mathrm{j}}^{(k)\text{-}1}$) whose inverse components are only either $\alpha^2 = 1/2$ or $\alpha^2 = 1$ in the cubic symmetry lattice material, is used. As shown in Fig. 4, the local strain in the truss member may be evaluated by the product of the applied uni-axial strain in the global coordinates and the linear transformation operator, e.g. $\varepsilon^{(1)} = \mathrm{A}_{11}^{(1)}\mathrm{E}_{11}$. By the local stress-strain relationship given by

$$\sigma^{(k)} = E_s^{(\mathrm{k})}\varepsilon^{(k)}, \tag{6}$$

where $E_s^{(k)}$ is Young's modulus of the k^{th} truss member, the relationship between the local stress and the global strain is

$$\sigma^{(k)} = E_s^{(k)}\mathrm{A}_{\mathrm{kl}}^{(k)}\mathrm{E}_{\mathrm{kl}} \tag{7}$$

Substituting Eq. (7) into Eq. (2), the macroscopic constitutive relationship ($\mathbf{\Sigma} = \mathbf{CE}$) is obtained

$$\Sigma_{\mathrm{ij}} = \sum_{k=1}^{K} v_{\mathrm{v}}^{(k)}E_s^{(k)}\mathrm{A}_{\mathrm{ij}}{}^{(k)}\mathrm{A}_{\mathrm{kl}}{}^{(k)}\mathrm{E}_{\mathrm{kl}} \tag{8}$$

Consequently, the macroscopic stiffness tensor **C** for the unit cell of a general lattice material is expressed as

$$\begin{aligned}\mathrm{C}_{\mathrm{ijkl}} &= \sum_{k=1}^{K} E_s^{(k)}v_{\mathrm{v}}^{(k)}\mathrm{A}_{\mathrm{ij}}{}^{(k)}\mathrm{A}_{\mathrm{kl}}{}^{(k)} \\ &= \sum_{k=1}^{K} E_s^{(k)}v_{\mathrm{v}}^{(k)}\left(\mathrm{a}_{\mathrm{i}}^{(k)} \cdot \mathrm{a}_{\mathrm{j}}^{(k)} \cdot \mathrm{a}_{\mathrm{k}}^{(k)} \cdot \mathrm{a}_{\mathrm{l}}^{(k)}\right)\end{aligned} . \tag{9}$$

Note that the macroscopic stiffness tensor is in the forth order tensor form [10, 17]

The continuum model of the open-cell foam is also based on the characteristic unit cell extracted from the open-cell cellular solids with randomly orientated struts. Moreover, the research concepts and approaches related to the open-cell foam structures have been accompanied with those related to the truss-lattice structures, in terms of interesting macro-micro scales, mechanical properties, constitutive model formation, and yield functions [18]. The bending mechanism can dominate the finite deformations of the randomly oriented struts within micro-cellular solid structures. By contrast, the contributions of the overall bending stiffness of the truss members periodically aligned are considered to be negligible, when compared with those of the axial stiffness [2, 11, 14]. Likewise, the plastic deformation at the connected nodes, shearing and torsion effect of individual truss members are not considered in the constitutive model. Using the tensor notation and subscripts (XX→11, YY→22, and ZZ→33 for axial direction

XY→12, XZ→13 and YZ→23 for shear direction), the macroscopic stress $\boldsymbol{\Sigma}$ and strain $\mathbf{E}$ are written in vector forms

$$\boldsymbol{\Sigma} = \left(\Sigma_{11}\ \Sigma_{22}\ \Sigma_{33}\ \Sigma_{12}\ \Sigma_{13}\ \Sigma_{23}\right)^{\mathrm{T}}, \tag{10}$$

$$\mathbf{E} = \left(\mathrm{E}_{11}\ \mathrm{E}_{22}\ \mathrm{E}_{33}\ \mathrm{E}_{12}\ \mathrm{E}_{13}\ \mathrm{E}_{23}\right)^{\mathrm{T}}. \tag{11}$$

Macro-scale shear strains are the total measurement of shear strain called the engineering strain in the surface plane (e.g. $\mathrm{E}_{12} = \mathrm{E}_{21}$, $\mathrm{E}_{13} = \mathrm{E}_{31}$, and $\mathrm{E}_{23} = \mathrm{E}_{32}$). Then, the macroscopic constitutive relationship written in the compact matrix form is

$$\begin{pmatrix}\Sigma_{11}\\ \Sigma_{22}\\ \Sigma_{33}\\ \Sigma_{12}\\ \Sigma_{13}\\ \Sigma_{23}\end{pmatrix} = \frac{E_s \pi r^2}{2\sqrt{2}L^2}\begin{pmatrix}\mathrm{C}_{1111} & \mathrm{C}_{1122} & \mathrm{C}_{1122} & 0 & 0 & 0\\ \mathrm{C}_{1122} & \mathrm{C}_{1111} & \mathrm{C}_{1122} & 0 & 0 & 0\\ \mathrm{C}_{1122} & \mathrm{C}_{1122} & \mathrm{C}_{1111} & 0 & 0 & 0\\ 0 & 0 & 0 & \mathrm{C}_{1212} & 0 & 0\\ 0 & 0 & 0 & 0 & \mathrm{C}_{1212} & 0\\ 0 & 0 & 0 & 0 & 0 & \mathrm{C}_{1212}\end{pmatrix}\begin{pmatrix}\mathrm{E}_{11}\\ \mathrm{E}_{22}\\ \mathrm{E}_{33}\\ \mathrm{E}_{12}\\ \mathrm{E}_{13}\\ \mathrm{E}_{23}\end{pmatrix} \tag{12}$$

where the non-dimensional parameters. C_{1111}, C_{1122}, and C_{1212} are given as follows:

For the octet unit cell (Case A);

$$\mathrm{C}_{1111} = 2 \tag{13a}$$

$$\mathrm{C}_{1122} = 1 \tag{13b}$$

$$\mathrm{C}_{1212} = 1 \tag{13c}$$

For the strengthened diagonal unit cell (Case B);

$$\mathrm{C}_{1111} = \left(2+\sqrt{2}\right)/2 \tag{14a}$$

$$\mathrm{C}_{1122} = 1/2 \tag{14b}$$

$$\mathrm{C}_{1212} = 1/2 \tag{14c}$$

For the strengthened octet unit cell (Case C);

$$\mathrm{C}_{1111} = 2+\sqrt{2} \tag{15a}$$

$$\mathrm{C}_{1122} = 1 \tag{15b}$$

$$\mathrm{C}_{1212} = 1 \tag{15c}$$

Note that the cross sectional area and Young's modulus of the solid truss member are identical in all truss members. Under the assumption of small deformation, if Young's modulus is replaced with a tangent modulus, this relationship will hold even when truss members undergo plastic deformation. The micro-scale elastic constitutive model is considered as the continuum system because component elastic constants possess the volume fractions of every single truss member. It is interesting to note that even though the stress state in every truss member is axial (tension or compression), shear stress and strain are induced in the equivalent continuum and the macroscopic constitutive matrix possesses nonzero shear stiffness ($\mathrm{C}_{1212} \neq 0$).

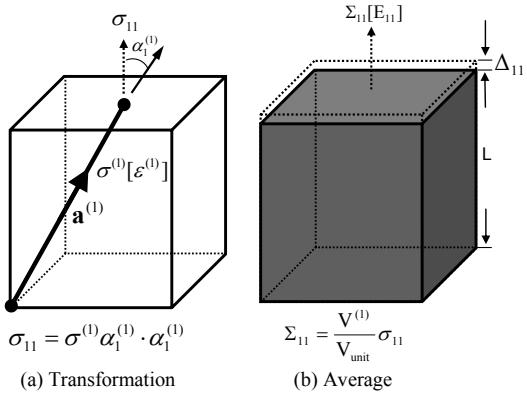

Fig. 4. Decomposition of homogenization procedures for the lattice materials.

3.3 The relative density

As mentioned above, the relative density ρ^* has a significant meaning and is a very useful parameter in interpreting the mechanically effective property of the lattice materials and estimating their lightweight effect. The relative density is defined as the ratio of the total volume that is occupied by all truss members in the unit cell to the volume of the unit cell element It should be noted that the relative density ρ^* includes the volume fractions (v_{v}) of individual truss members and the macroscopic stiffness ($\mathbf{C} = \sum E_s v_{\mathrm{v}} \mathbf{A}^{\mathrm{T}}\mathbf{A}$) [10, 17]. Thus, it is the sum of the volume fraction of all composing members.

$$\rho^* = \sum_{k=1}^{K} v_{\mathrm{v}}^{(k)} = \frac{3\mathrm{C}_{1111} + 6\mathrm{C}_{1122}}{E_s} \tag{16a}$$

Thus, the specific values of relative densities are as follows:
Octet unit cell element -Case A;

$$\rho^* = 3\sqrt{2}\pi \mathrm{r}^2/\mathrm{L}^2 \tag{16b}$$

Strengthened diagonal unit cell element - Case B;

$$\rho^* = \left(6\sqrt{2}+3\right)\pi \mathrm{r}^2/4\mathrm{L}^2 \tag{16c}$$

Strengthened octet unit cell element - Case C;

$$\rho^* = \left(3\sqrt{2}+3\right)\pi \mathrm{r}^2/\mathrm{L}^2 \tag{16d}$$

The relative density is a useful parameter in optimizing the effective elastic moduli (typ. E^* and G^*) of a lattice material subjected to the weight constraint. For example, in Fig. 5, the effective elastic moduli for three unit cell elements are shown for increasing the relative density, which is proportional to $(\mathrm{r}/\mathrm{L})^2$. With the increase of the relative density, relative elastic modulus ratios E^*/E_s and G^*/E_s increase rapidly. Even though r/L is the same in three unit cells, the relative densities ρ^* are quite different due to the different packing systems as shown in Fig. 3. When $\mathrm{r}/\mathrm{L} = 0.1$, the strengthened

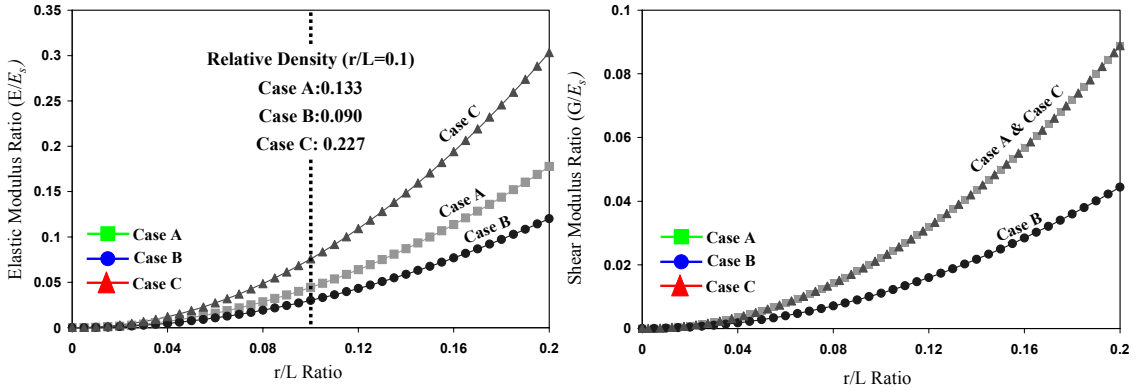

Fig. 5. Comparisons of elastic moduli for the unit cells with cubic symmetry.

octet unit cell element has the highest relative density, $\rho^* = 0.227$. The highest strength among three unit cell element is also expected at this unit cell element. It is interesting to note that the shear modulus ratio G^*/E_s in octet unit cell element (Case A) and strengthened octet unit cell element (Case C) is identical (see Fig. 5(b)) in spite of the different relative density. This is because the bending response, which occurs at the cubic-lattice member due to the global shear force, does not make any contribution to the formation of the effective elastic shear modulus. It is associated with the stretching response at the truss members.

3.4 Small stress-strain formulation with micro-macro transformation

Since the continuum properties of the unit cell structures are influenced by the mechanical properties of component truss members, the stress-strain relationship between micro-scale and macro-scale is predicted from the effective constitutive relationship ($\mathbf{\Sigma} = \mathbf{CE}$).

Here, we briefly examine the relationships between macro-scale and micro-scale strain for truss members and between the macro-scale stress and the macro-scale strain. The small-strain formulation for one dimensional truss member in the micro-scale level is established by the superposition of transformed total applied stains in the macro-scale level. For the verification of this strain formulation, two dimensional truss lattice materials (diagonal- and octet-truss members) under multi-axial loading ($E_{11}+E_{22}$ and $E_{22}+E_{12}$) are presented in Fig. 6. Macro-scale strains under the displacement loading control are applied to each nodal point in the unit cell element. Recall that the relation between the unit vectors $\mathbf{a}^{(k)}$ and the common vector components $\alpha^{(k)}$ are summarized in Table 1.

We note that overall member strain as well as local stress continuously increases at truss members subjected to either out-of-perpendicular or parallel stretching [19, 20]. These truss members are denoted by "||" on the red-colored struts (see Fig. 6). Those truss members aligned with normal direction to the applied strain E_{ij} are deformed mostly by the plastic hinge due to the bending effect. For multi-loading cases, the micro-scale strain is obtained by the sum of applied strains, with the coordinate transformed. The macro-micro strain relationship is defined by:

For multi-axial loading $E_{11}+E_{22}$ (Fig. 6(a));

$$\varepsilon^{(1)} = A_{11}^{(1)}E_{11} + A_{22}^{(1)}E_{22} = (\alpha^{(oct)})^2(E_{11}+E_{22}) \quad (17a)$$

$$\varepsilon^{(2)} = A_{11}^{(2)}E_{11} + A_{22}^{(2)}E_{22} = (\alpha^{(oct)})^2(E_{11}+E_{22}) \quad (17b)$$

$$\varepsilon^{(3)} = A_{11}^{(3)}E_{11} + A_{22}^{(3)}E_{22} = (\alpha^{(cub)})^2(E_{22}) \quad (17c)$$

$$\varepsilon^{(4)} = A_{11}^{(4)}E_{11} + A_{22}^{(4)}E_{22} = (\alpha^{(cub)})^2(E_{11}) \quad (17d)$$

$$\varepsilon^{(5)} = A_{11}^{(5)}E_{11} + A_{22}^{(5)}E_{22} = (\alpha^{(cub)})^2(E_{11}) \quad (17e)$$

For multi-axial loading $E_{22}+E_{12}$ (Fig. 6(b));

$$\varepsilon^{(1)} = A_{22}^{(1)}E_{22} + A_{12}^{(1)}E_{12} = (\alpha^{(oct)})^2(E_{22}-E_{12}) \quad (18a)$$

$$\varepsilon^{(2)} = A_{22}^{(2)}E_{22} + A_{12}^{(2)}E_{12} = (\alpha^{(oct)})^2(E_{22}+E_{12}) \quad (18b)$$

$$\varepsilon^{(3)} = A_{22}^{(3)}E_{22} = (\alpha^{(cub)})^2(E_{22}) \quad (18c)$$

$$\varepsilon^{(4)} = A_{22}^{(4)}E_{22} = 0 \quad (18d)$$

$$\varepsilon^{(5)} = A_{22}^{(5)}E_{22} = 0 \quad (18e)$$

The localized stress of the truss member is formulated by the 1D stress-strain constitutive function for the solid basis truss model such as $\sigma^{(k)} = \sigma[\varepsilon^{(k)}]$. By using the stress average (Eq. (2)) and macro-micro strain relationships (Eq. (4)), uni-axial stresses at the macro-scale level are derived as follows:

For uni-axial loading E_{22} ;

$$\begin{aligned}\Sigma_{22} = {} & 2\nu_v^{(oct)}(\alpha^{(oct)})^2\sigma[(\alpha^{(oct)})^2E_{22}] \\ & + \nu_v^{(cub)}(\alpha^{(cub)})^2\sigma[(\alpha^{(cub)})^2E_{22}]\end{aligned} \quad (19)$$

For uni-axial loading E_{12} ;

$$\begin{aligned}\Sigma_{12} = {} & \nu_v^{(oct)}(\alpha^{(oct)})^2\sigma[(\alpha^{(oct)})^2(E_{12})] \\ & - \nu_v^{(oct)}(\alpha^{(oct)})^2\sigma[(\alpha^{(oct)})^2(-E_{12})]\end{aligned} \quad (20)$$

In multi-axial cases, two dimensional macro-scale plane stress components such as Σ_{11} and Σ_{22} are generated in terms of the applied loading strains, e.g. E_{11} and E_{22}. One dimen-

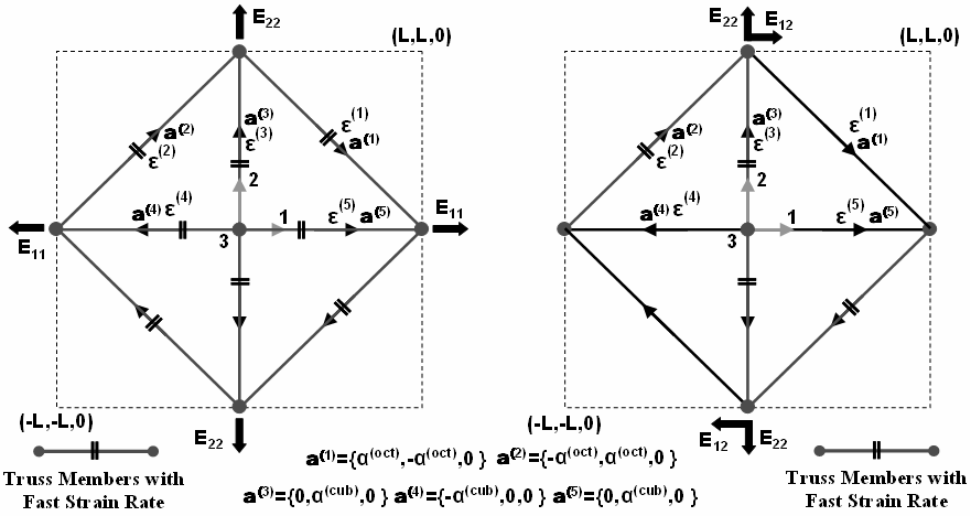

(a) Multi-axial loading case (E11+E22) (b) Multi-axial loading case (E22+E12)

Fig. 6. Macro-micro strain formation of 2D truss-lattice materials under multi-axial loading.

sional micro-scale strain of the truss member is simultaneously affected by applied strain loads such that $\varepsilon^{(k)} = A_{11}^{(k)}E_{11} + A_{22}^{(k)}E_{22}$. As a result, the strength contribution from one dimensional truss member subjected to stretching is also simultaneously distributed into loading directions. If micro-scale strain is fixed to the certain level of the strain value such as $\varepsilon^{(k)} = A_{11}^{(k)}E_{11} + A_{22}^{(k)}E_{22} = \varepsilon^{o}$, the sum of macro-scale stress components, Σ_{11} and Σ_{22}, is constant. Therefore, the stress functions on the 2D surface plane under multi-axial loads are formulated as:

For multi-axial loading $E_{11} + E_{22}$ (Fig. 6(a));

$$\begin{aligned}&\Sigma_{11} + \Sigma_{22} = 2\nu_v^{(oct)}(\alpha^{(oct)})^2\sigma[(\alpha^{(oct)})^2(E_{11} + E_{22})]\\&+\nu_v^{(cub)}(\alpha^{(cub)})^2\sigma[(\alpha^{(cub)})^2E_{11}]\\&+\nu_v^{(cub)}(\alpha^{(cub)})^2\sigma[(\alpha^{(cub)})^2E_{22}]\end{aligned} \tag{21}$$

For multi-axial loading $E_{22} + E_{12}$ (Fig. 6(b));

$$\begin{aligned}&\Sigma_{22} + \Sigma_{12} = \nu_v^{(oct)}(\alpha^{(oct)})^2\sigma[(\alpha^{(oct)})^2(E_{22} + E_{12})]\\&+\nu_v^{(oct)}(\alpha^{(oct)})^2\sigma[(\alpha^{(oct)})^2(E_{22})]\\&-\nu_v^{(oct)}(\alpha^{(oct)})^2\sigma[(\alpha^{(oct)})^2(-E_{12})]\\&+\nu_v^{(cub)}(\alpha^{(cub)})^2\sigma[(\alpha^{(cub)})^2E_{22}]\end{aligned} \tag{22}$$

In order to derive uni-axial stress from Eqs. (21) and (22), one of the applied macro-scale strains should be set as zero. For instance, if E_{11} is zero in Eq. (21), this stress function reduces to the uni-axial stress case as shown in Eq. (19).

Finally, the micro-scale stress states of the component truss member are directly joined to the macro-scale stress associated with its transformation and volume fraction ($\mathbf{\Sigma} = \sum \nu_v \sigma \mathbf{A}$). Thus, macro-scale stress surface functions are applied to examine the stress state of truss members, which includes plastic stress as well as elastic stress.

The plastic flow rule is also satisfied at the macro-scale level. We also obtain the plastic strain using the linear combination of the transformation vector

$$E_{ij}^{P} = A_{ij}^{(k)-1}\varepsilon_{P}^{(k)}. \tag{23}$$

The total strain consists of the sum of the elastic strain and plastic strain, i.e.

$$\mathbf{E} = \mathbf{E}^{E} + \mathbf{E}^{p}. \tag{24}$$

The elastic stress-strain relationship at the macro-scale level is formulated by using the macro-scale plastic strain $\mathbf{E}^{P}$ [21] as follows:

$$\mathbf{\Sigma} = \mathbf{C}\left(\mathbf{E} - \mathbf{E}^{P}\right) \tag{25}$$

Finally, we obtain the constitutive equations as the tensorial form

$$\begin{aligned}\Sigma_{ij} &= \sum_{k=1}^{n} C_{ijkl}^{(k)}(E_{kl} - E_{kl}^{P})\\&= \sum_{k=1}^{n} E_s \nu_V^{(k)} A_{ij}^{(k)} A_{kl}^{(k)}(E_{kl} - E_{kl}^{P})\end{aligned}. \tag{26}$$

In the next section, (1) the small-strain formulation, (2) analytical stress function, and (3) stress-stain relationship at the macro-scale level presented in this study will be verified with the numerical experiment performed by the FE program [22].

4. Numerical calculations and discussion

4.1 FE models and calculations

The material property models of the solid-basis truss members are summarized in Fig. 7. A previous study of lattice materials [2, 14, 23] accepted the perfectly elasto-plastic

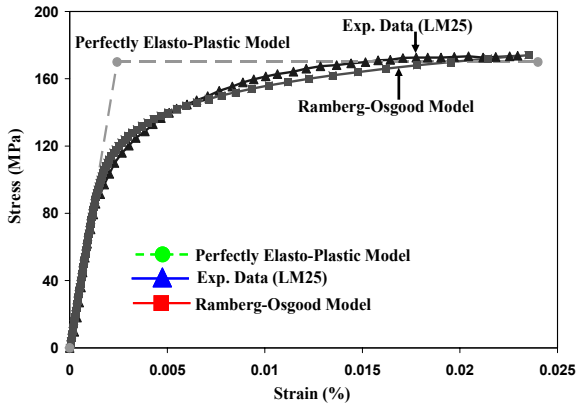

Fig. 7. Stress-strain relationships at the microscopic level.

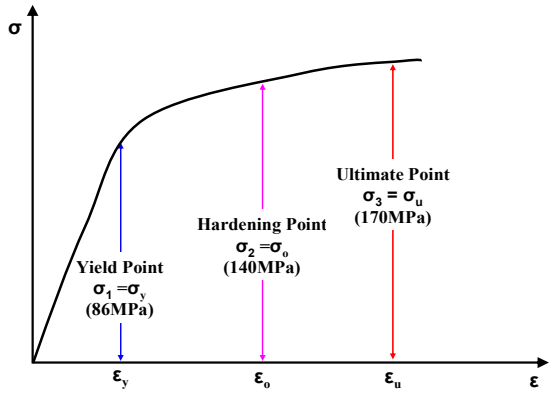

Fig. 8. The performance levels of micro-scale stress for the plastic models.

model. The mechanism-based multi-surface plastic models under the use of this material model were developed to represent the complex behavior of lattice solids. However, the exact expression to simulate the plastic behavior of these materials was restricted due to the approximate material models used for discrete truss members.

Numerical tests were performed by using nonlinear finite element (FE) program ABAQUS [22]. The material property of LM 25 aluminum (Blue dotted line shown in Fig. 7) measured by the uni-axial pull test was assigned with FE models for unit cells. The behavior of LM 25 was simulated by the Ramberg-Osgood model (Red dotted line shown in Fig. 7) in order to apply the accurate material model to analytical predictions for the macro-scale stress surface. The stress-strain constitutive law for the truss member at the micro-scale level was employed in the analytical predictions as follows:

Ramberg-Osgood model;

$$\varepsilon = \frac{\sigma}{E_s} + \frac{\alpha\sigma_s}{E_s}\left(\frac{\sigma}{\sigma_s}\right)^n \tag{27}$$

where σ_s / E_s indicates the elastic strain and $\alpha\sigma_s / E_s$ indicates the yield offset typically taken as the value of 0.002. The power coefficient n was assumed to be 8.9. The elastic

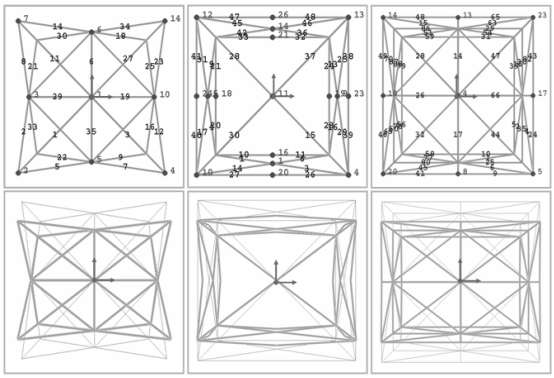

Fig. 9. FE modeling for unit cells (Top) and exaggerated deformation (Bottom).

modulus E_s and the ultimate stress σ_u were taken equal to 70 GPa and 170 MPa, respectively.

The plastic domain of the yield stress surface at the macro-scale level was investigated through the analytical predictions and FE test results at the stress performance level. The stress performance level shown in Fig. 8 consists of the yield point ($\sigma_y = 86$ MPa), hardening point ($\sigma_o = 140$ MPa), and ultimate point ($\sigma_u = 170$ MPa) for the micro-scale stress of the truss members. During the loading test performed on FE models, the axial stresses denoted by "S11" at the ABAQUS program were measured by using the field out-put commend at all time steps [22].

In the FE models for cubic-symmetric unit cells, each truss member having a cylindrical shape was modeled by the quadratic beam element (B32 element in the ABAQUS program). The cross section and material property of truss members were assigned into this element. For the purpose of avoiding the rigid body motion and rotation, some edge points at the end tips of structures were constrained. FE models and exaggerate deformations are illustrated in Fig. 9. The uniform loads based on the displacement control were applied to highlighted nodal points in red at the same surface. Multi-axial loads with the same loading strain rates (e.g. $\left|E_{ii}/E_{jj}\right| = 1$ and $\left|E_{ij}/E_{ii}\right| = 1$) as well as with uni-axial loads (e.g. $\left|E_{ii}/E_{jj}\right| = 0$ or ∞ and $\left|E_{ij}/E_{ii}\right| = 0$ or ∞) were applied to FE models. The macro-scale stresses were obtained by the constitutive relationship (see Eqs. 12 and 43) after FE tests.

The values of the applied forces were automatically calculated by using the history out-put commend in the ABAQUS program. For the small-strain formulation, the geometric linearity or first order analysis was applied during FE tests. The stress of the cylindrical strut and the strain of the unit cell were obtained by these numerical tests. The macro-scale stresses were computed by substituting these strains at the specific micro-scale stress level into the constitutive equations.

4.2 Plastic stress surface

The analytical prediction for the macro-scale stress surface was derived by the macro-scale and micro-scale stress relationship shown in Eq. (2). Recalling Sec. (3.4) allows us to

formulate the analytical stress surface. The applied macro-scale strain on the global coordination is rotated into the micro-scale one with the linear transformation operator (refer to Eq. (4)). Within the small-strain formulation, the micro-scale strain $\varepsilon^{(k)}$ is predicted from the applied macro-scale strain $\mathbf{E}$ using the geometric linear transformation due to the unit vector $\mathbf{a}$. Similarly, the stress state of the truss member is also calculated by using the stress-strain relationship in the micro-scale level (see Fig. 7). The analytical predictions to estimate the macro-scale stress state $\mathbf{\Sigma}$ were denoted by the micro-scale stress $\sigma^{(k)}$ as the internal variable. The extension of the stress surface due to the plastic deformation of the truss members are investigated in this section, as compared analytical predictions with FE test results at the performance level of micro-scale stress. It is also shown that the relative density can be obtained by the summation of uni-axial stresses derived from the analytical predictions.

4.2.1 Plastic stress surface for the octet unit cell (Case A Model)

For the octet unit cell (Case A), all truss members were aligned with the common unit vector component ($\alpha^{(oct)} = \sqrt{2}/2$). Thereby, the truss members on the same stress plane surface include the same strain or strain rate. In addition, regular stress-shape modes occurred at the surface of the unit cell element under the multi-axial loads. The analytical predictions at each performance stress level (i.e. yield, hardening, and ultimate state) were derived to determine the analytical stress function in the macro-scale stress surface

Basic equation: $|\Sigma_{ii}| + |\Sigma_{jj}| = 2\nu_v^{(oct)}\sigma^{(oct)}$
(ii-jj stress surface, e.g. (Σ_{11}, Σ_{22}))
$|\Sigma_{ii}| + 2|\Sigma_{ij}| = 2\nu_v\sigma^{(oct)}$
(ii-ij stress surface e.g. (Σ_{11}, Σ_{12})), (28a)

where micro-scale strain and stress of the truss member in the octet unit cell element ($\varepsilon^{(oct)}$ and $\sigma^{(oct)}$) are substituted into

1D yield state: $\varepsilon^{(oct)} = \varepsilon_y$ and $\sigma^{(oct)} = \sigma[\varepsilon_y]$ (28b)

1D stain hardening state: $\varepsilon^{(oct)} = \varepsilon_o$ and $\sigma^{(oct)} = \sigma[\varepsilon_o]$ (28c)

1D ultimate state: $\varepsilon^{(oct)} = \varepsilon_u$ and $\sigma^{(oct)} = \sigma[\varepsilon_u]$ (28d)

according to the micro-scale stress state. Constitutive equations for an 1D truss member (simulated by the Ramberg-Osgood model) were assigned into the analytical stress function. The general volume fraction for each truss member embedded in the infinitive unit cell volume is given by the equation

$$\nu_v = \frac{\sqrt{2}A_o L}{2V_{unit}} = \frac{\sqrt{2}\pi}{2}\left(\frac{r}{L}\right)^2 . \quad (29)$$

The relative density ρ^* was taken as 0.133.

Comparisons between the analytical predictions and FE test results for the octet unit cell element and various stress-shape modes are illustrated in Fig. 10. The macro-scale stress $\mathbf{\Sigma}$ is normalized by the yield stress for the solid basis material σ_y. Mises stress-plots during static analyses, which occur with continuous displacement-load increments, are anchored around the stress surface. The uni-axial stresses are located on the interceptions of the stress surface, and stress surface are enclosed by interpolating two uni-axial stress points. The truss members with the performance stress levels in the micro-scale (see Fig. 8) are denoted by "||" on the red contour of Mises stress plots. As increasing applied strain loading, micro-scale strain also increases at these truss members. The stress-shape modes determined by these truss members are dependent on the loading combinations such as tension-tension (← →) and compression-compression (→ ←). As shown in Fig. 10, the identical stress-shape modes exist between completely opposite load combinations (e.g. compression-compression (C-C) vs. tension-tension (T-T)). The stress surfaces are extended as increasing the plastic deformation of the truss members with strain hardening effect. It is noted from Fig. 10 that all results show good agreements between FE test results and analytical predictions.

To discuss the relative density of the lattice material ρ^*, the hydrostatic stress was introduced to the stress surface. The macro-scale stress function in the 3D domain and the failure state of the unit cell element subjected to the hydrostatic pressure are illustrated in Fig. 11. All truss members fail simultaneously under the hydrostatic pressure. All interpolated lines from the interception on the macro-scale uni-axial stress intersect in the hydrostatic pressure points, H1 (under tensile pressure) and H2 (under compression pressure). All macro-scale uni-axial stresses Σ_{11}, Σ_{22}, and Σ_{33} include the volume fraction of the individual truss member $\nu_v^{(k)}$. Therefore, we can calculate the relative density at the state of the hydrostatic pressure by summation of all uni-axial stress components as follow

$$\rho^* = 3\frac{(\Sigma_{11} + \Sigma_{22} + \Sigma_{33})}{\sigma^{(oct)}} = 3\sqrt{2}\pi\left(\frac{r}{L}\right)^2 . \quad (30)$$

This relative density is identical to Eq. (16b) from constitutive equations.

4.2.2 Plastic stress surface for the strengthened diagonal unit cell (Case B Model)

The strengthened diagonal unit cell element (Case B) consists of two different sub-lattice elements, the diagonal-lattice element and the cubic-lattice element, as shown in Fig. 3(c). Thus, two different unit direction vectors exist in this type of unit cell structure. The truss members in the cubic-lattice element were transformed with the unit direction vectors parallel to the global axes for the axial loads ($\alpha^{(cub)} = 1$). This structural arrangement for truss members provides the principal axial stiffness to the constitutive equations. The axial strength is significantly upgraded due to the cubic-lattice members.

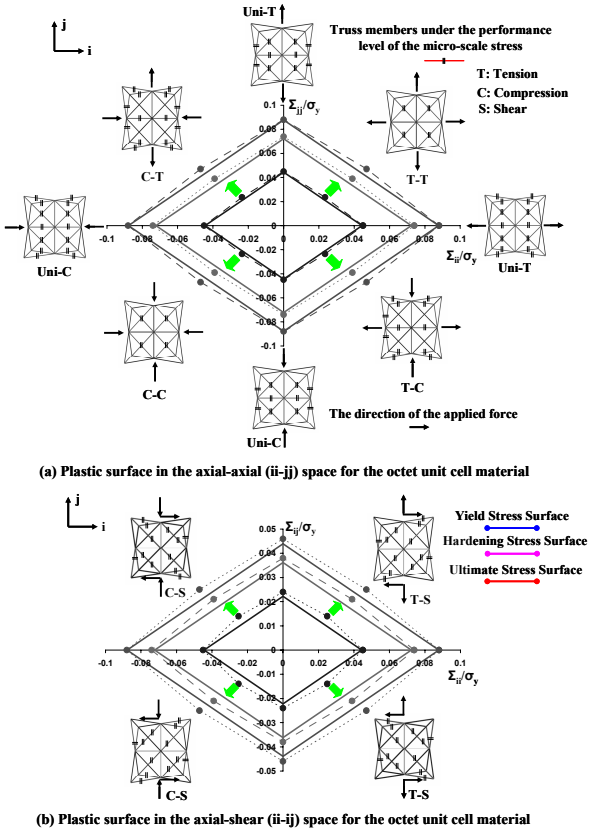

Fig. 10. Comparison between FE test results (Dash-lines) and analytical predictions (Solid-lines) for the extension of the stress surface according to the performance stress levels based on the micro-scale stress (Octet unit cell element).

However, strut members parallel to the axial loads are susceptible to the plastic failure because of the fast strain rate. In other words, truss members in the cubic-lattice element possess faster strain flow rate than those in the diagonal-lattice element. The relationships between micro-scale and macro-scale strains are summarized by the following:

Truss members in the cubic-lattice element;

$$\varepsilon^{(cub)} = \mathrm{A}_{ij}^{(cub)}\mathrm{E}_{ij} \tag{31a}$$

Truss members in the diagonal-lattice element;

$$\varepsilon^{(dia)} = \mathrm{A}_{ij}^{(dia)}\mathrm{E}_{ij}\,. \tag{31b}$$

The strain for truss members in the cubic unit cell element is simplified by substituting Eq. (31b) into Eq. (31a) as follows:

$$\varepsilon^{(cub)} = \frac{\mathrm{A}_{ij}^{(cub)}}{\mathrm{A}_{ij}^{(dia)}}\varepsilon^{(dia)} = \left(\frac{\alpha^{(cub)}}{\alpha^{(dia)}}\right)^2 \varepsilon^{(dia)} \tag{32}$$

The analytical predictions at each performance stress level were derived to determine the analytical stress function in the macro-scale stress surface as follows

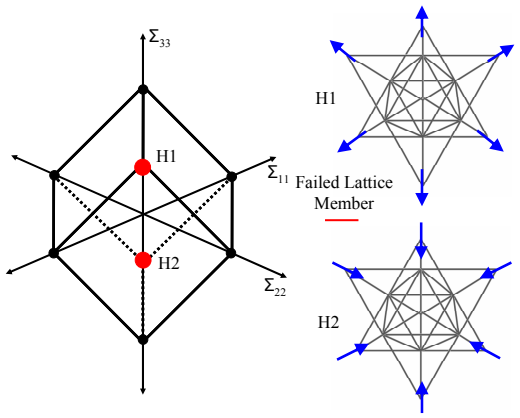

Fig. 11. Failure states at the octet unit cell under the hydro-static pressure.

Basic equation:

$$\left|\Sigma_{ii}\right| + \left|\Sigma_{jj}\right| = \nu_{\mathrm{v}}^{(dia)}\sigma^{(dia)} + \nu_{\mathrm{v}}^{(cub)}\sigma^{(cub)}$$

(ii-jj stress surface)

$$\left(\frac{\Sigma_{ii}}{\nu_{\mathrm{v}}^{(dia)}\sigma^{(dia)} + \nu_{\mathrm{v}}^{(cub)}\sigma^{(cub)}}\right)^2 + \left(\frac{2\Sigma_{ij}}{\nu_{\mathrm{v}}^{(dia)}\sigma^{(dia)}}\right)^2 = 1$$

(ii-ij stress surface). (33a)

Internal variables from both component sub-lattice elements such as micro-scale stress and volume fraction are found in the analytical prediction. The bending effect happening at the cubic-lattice member due to the shear force was negligible in comparison with the stretching effect. As a result, the macro-scale stress function in ii-ij surface (e.g. (Σ_{11},Σ_{12})), was formulated as the elliptical form. Using the constitutive equation function for the 1D truss member ($\sigma^{(k)} = \sigma[\varepsilon^{(k)}]$), the micro-scale stress-strain relationships for both diagonal-truss members ($\varepsilon^{(dia)}$ and $\sigma^{(dia)}$) and cubic-truss members ($\varepsilon^{(cub)}$ and $\sigma^{(cub)}$) are converted into

1D Yield State: $\varepsilon^{(dia)} = \varepsilon_y$, $\sigma^{(dia)} = \sigma[\varepsilon_y]$,

and $\sigma^{(cub)} = \sigma\left[(\alpha^{(cub)}/\alpha^{(dia)})^2\varepsilon_y\right]$ (33b)

1D Strain Hardening: $\varepsilon^{(dia)} = \varepsilon_o$, $\sigma^{(dia)} = \sigma[\varepsilon_o]$,

and $\sigma^{(cub)} = \sigma\left[(\alpha^{(cub)}/\alpha^{(dia)})^2\varepsilon_o\right]$ (33c)

1D Ultimate State: $\varepsilon^{(dia)} = \varepsilon_u$, $\sigma^{(dia)} = \sigma[\varepsilon_u]$,

and $\sigma^{(cub)} = \sigma\left[(\alpha^{(cub)}/\alpha^{(dia)})^2\varepsilon_u\right]$. (33d)

The general volume fractions for each truss member are given to below

$$\nu_{\mathrm{v}}^{(dia)} = \frac{\sqrt{2}\mathrm{A_o L}}{2\mathrm{V_{unit}}} = \frac{\sqrt{2}\pi}{2}\left(\frac{\mathrm{r}}{\mathrm{L}}\right)^2 \tag{34a}$$

$$\nu_{\mathrm{v}}^{(cub)} = \frac{\mathrm{A_o L}}{4\mathrm{V_{unit}}} = \frac{\pi}{4}\left(\frac{\mathrm{r}}{\mathrm{L}}\right)^2\,. \tag{34b}$$

Comparison between the analytical predictions and FE test

results is shown in Fig. 12 for $\rho^* = 0.090$. The stress-shape modes under the combination of applied loads are also illustrated in the plan view of the unit cell element. Similar to the octet unit cell, the relative density is computed at the state of the hydrostatic pressure

$$\rho^* = \frac{3\sqrt{2}}{2}\pi\left(\frac{\mathrm{r}}{\mathrm{L}}\right)^2 + \frac{3}{4}\pi\left(\frac{\mathrm{r}}{\mathrm{L}}\right)^2 . \tag{35}$$

This relative density is also identical to Eq. (16c).

4.2.3 Plastic stress surface for the strengthened octet unit cell (Case C Model)

The strengthened octet unit cell element (Case C) consists of an octet unit cell element and cubic-lattice elements as shown in Fig. 3(d). The truss members in the octet unit cell element were aligned with the same transformation angle to the axes. Two different transformation angles, which are inclined ($\alpha^{(oct)} = \sqrt{2}/2$) or parallel ($\alpha^{(cub)} = 1$) to the axes, exist in this type of unit cell element. Similar to the strengthened diagonal unit cell element (Case B), the strain rates of the truss members in the cubic-lattice elements flow more quickly in comparison with those of the truss members in the octet unit cell element. As a result, the first yield σ_y or the first ultimate state σ_u generally occurs at truss members in the cubic-lattice elements due to the fast strain rates. The relationships between micro-scale and macro-scale strains are defined by Truss members in the cubic-lattice element:

$$\varepsilon^{(cub)} = \mathrm{A}_{\mathrm{ij}}^{(cub)}\mathrm{E}_{\mathrm{ij}} \tag{36a}$$

Truss members in the octet-lattice element:

$$\varepsilon^{(oct)} = \mathrm{A}_{\mathrm{ij}}^{(oct)}\mathrm{E}_{\mathrm{ij}} . \tag{36b}$$

The strain of the truss members in the cubic-lattice elements ($\varepsilon^{(cub)}$) can be converted into

$$\varepsilon^{(cub)} = \frac{\mathrm{A}_{\mathrm{ij}}^{(cub)}}{\mathrm{A}_{\mathrm{ij}}^{(\mathrm{oct})}}\varepsilon^{(oct)} = \left(\frac{\alpha^{(cub)}}{\alpha^{(oct)}}\right)^2 \varepsilon^{(oct)} . \tag{37}$$

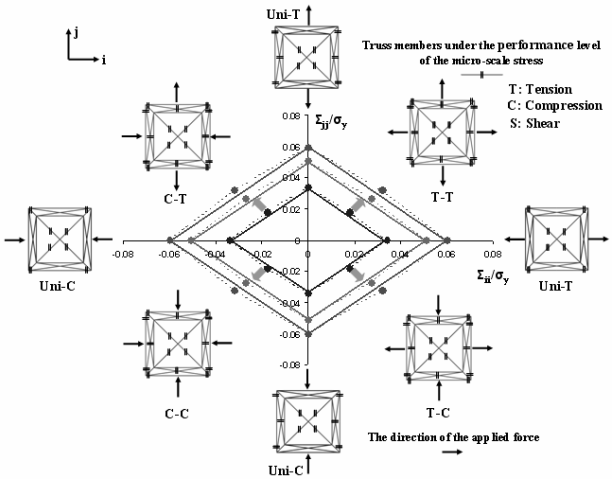

(a) Plastic surface is the axial-axial (ii-jj) space for diagonally strengthened cubic unit cell material

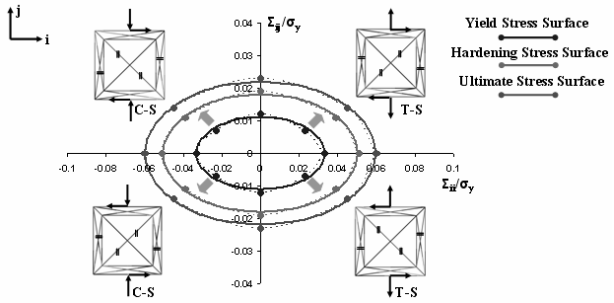

(b) Plastic surface in the axial-shear (ii-jj) space for diagonally strengthened cubic unit cell material

Fig. 12. Comparison between FE test results (Dash-lines) and analytical predictions (Solid-lines) for the extension of the stress surface extension according to the performance stress levels based on the micro-scale stress (Strengthened diagonal unit cell element).

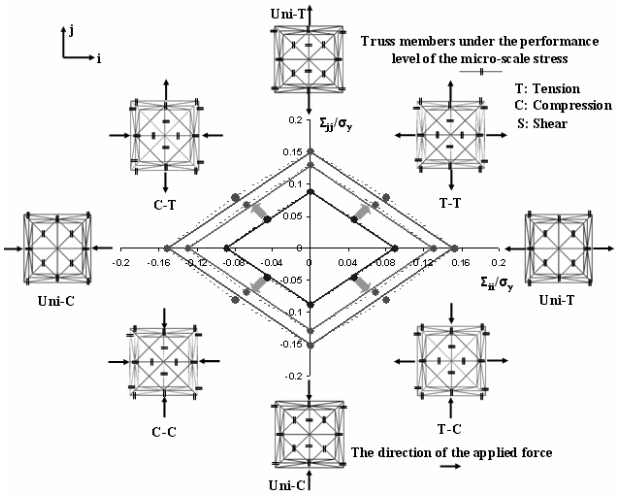

(a) Plastic surface is the axial-axial (ii-jj) space for strengthened octet-cubic unit cell material

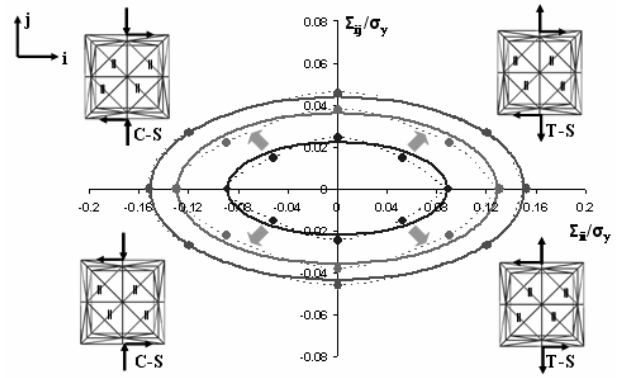

(b) Plastic surface in the axial-shear (ii-jj) space for strengthened octet unit cell material

Fig. 13. Comparison between FE test results (Dash-lines) and analytical predictions (Solid-lines) for the extension of the stress surface according to the performance stress levels based on the micro-scale stress (Strengthened octet unit cell element).

The analytical predictions at each performance stress level were derived by
Basic equation:

$$\left|\Sigma_{ii}\right| + \left|\Sigma_{jj}\right| = 2v_v^{(oct)}\sigma^{(oct)} + 4v_v^{(cub)}\sigma^{(cub)}$$

(ii-jj stress surface)

$$\left(\frac{\Sigma_{ii}}{2v_v^{(oct)}\sigma^{(oct)} + 4v_v^{(cub)}\sigma^{(cub)}}\right)^2 + \left(\frac{\Sigma_{jj}}{v_v^{(oct)}\sigma^{(oct)}}\right)^2 = 1$$

(ii-ij stress surface). (38a)

Micro-scale strain-stress relationships for both octet-truss members ($\varepsilon^{(oct)}$ and $\sigma^{(oct)}$) and cubic- truss members ($\varepsilon^{(cub)}$ and $\sigma^{(cub)}$) are converted into

1D Yield State: $\varepsilon^{(oct)} = \varepsilon_y$, $\sigma^{(oct)} = \sigma[\varepsilon_y]$,

and $\sigma^{(cub)} = \sigma\left[(\alpha^{(cub)}/\alpha^{(oct)})^2 \varepsilon_y\right]$ (38b)

1D Strain Hardening: $\varepsilon^{(oct)} = \varepsilon_o$, $\sigma^{(oct)} = \sigma[\varepsilon_o]$,

and $\sigma^{(cub)} = \sigma\left[(\alpha^{(cub)}/\alpha^{(oct)})^2 \varepsilon_o\right]$ (38c)

1D Ultimate State: $\varepsilon^{(oct)} = \varepsilon_u$, $\sigma^{(oct)} = \sigma[\varepsilon_u]$,

and $\sigma^{(cub)} = \sigma\left[(\alpha^{(cub)}/\alpha^{(oct)})^2 \varepsilon_u\right]$. (38d)

The general volume fractions for octet- and cubic-truss members are as follows

$$v_v^{(oct)} = \frac{\sqrt{2}A_o L}{2V_{unit}} = \frac{\sqrt{2}\pi}{2}\left(\frac{r}{L}\right)^2 \quad (39a)$$

$$v_v^{(cub)} = \frac{A_o L}{4V_{unit}} = \frac{\pi}{4}\left(\frac{r}{L}\right)^2 . \quad (39b)$$

The volume fraction of the octet-truss member is identical to that of the diagonal-truss member shown in Eq. (34a). Similarly, the relative density of this unit cell element is calculated as follows

$$\rho^* = 3\sqrt{2}\pi\left(\frac{r}{L}\right)^2 + 3\pi\left(\frac{r}{L}\right)^2 . \quad (40)$$

Comparison between the analytical predictions and FE test results and various stress-shape modes are illustrated in Fig. 13 for $\rho^* = 0.227$. A couple of stress-shape modes also exist between opposite-load combinations on the macro-scale stress surface (compression-compression (C-C) vs. tension-tension (T-T)). This unit cell element is relatively denser than other two unit cell elements within the unit volume space. Therefore, the strengthened octet unit cell element can hold the largest envelop of the stress surface among three unit cell elements. So, we have $\Sigma_{ii}/\sigma_y = \Sigma_{jj}/\sigma_y = 0.151$ at the ultimate stress surface, when $\rho^* = 0.227$. Good agreements in the stress plots confirm the accuracy and adequacy of the analytical predictions for the macro-scale stress surface.

5. Concluding summary

Analytical predictions and FE tests are performed to understand the effective mechanical properties and behaviors of the unit cells with cubic symmetry beyond the elastic regime. The packing characteristic, relative density, stiffness contribution, and component unit cell elements are analyzed for tailoring the elastic constant stiffness tensor in the equivalent continuum model. The local stresses in the truss members (at the micro-scale level) are homogenized in the unit volume space considering the volume fractions of discrete truss members. In such a homogenization process, the relationships between micro-scale and micro-scale variables are established.

The continuum-based plasticity models for the cubic-symmetric lattice materials subjected to the multi-axial loads are also investigated through the analytical and FE studies. The analytical expressions that determine the macro-scale stress surface are given in terms of the local stresses in the discrete truss members. The strain hardening material model was used in the plastic formulation at the micro-scale level. As increasing the strain of truss members, the macro-scale stress surfaces show the expansion due to the hardening material effect of the internal truss members. Finally, the adequacy and propriety of analytical predictions are clearly verified through comparisons together with the results of FE analyses and the theoretical calculations of relative densities.

Acknowledgements

This research was supported by WCU (World Class University) program through the National Research Foundation of Korea funded by the Ministry of Education, Science and Technology (R32-2008-000-20042-0). The authors also gratefully acknowledge the helpful advices of Professor D. L. McDowell.

References

[1] R. Biagi and H. Bart-Smith, Imperfection sensitivity of pyramidal core sandwich structures, *International Journal of Solids and Structures,* 44 (2007) 4690-4706.

[2] V. S. Deshpande, N. A. Fleck and M. F. Ashby, Effective properties of the octet-truss lattice material. *Journal of the Mechanics and Physics of Solids,* 49 (2001) 1747-1769.

[3] A. G. Evans, J. W. Hutchinson, N. A. Fleck, M. F. Ashby and H. N. G. Wadley, The topological design of multifunctional cellular metals. *Progress in Material Science,* 46 (2001) 309–327.

[4] J. S. Liu and T. J. Lu, Multi-objective and multi-loading optimization of ultra lightweight truss materials. *International Journal of Solids and Structure,* 41 (2004) 619-635.

[5] T. J. Liu, Z. C. Deng and T. J. Lu, Design optimization of truss-cored sandwiches with homogenization, *International Journal of Solids and Structure,* 43 (2006) 7891-7918.

[6] R. M. Christensen, Mechanics of cellular and other low-

density materials, *International Journal of Solids and Structure,*. 37 (2000) 93-104.

[7] M. Doyoyo and J. W. Hu, Plastic failure analysis of an Auxetic foam or inverted strut lattice under longitudinal and shear loads, *Journal of the Mechanics and Physics of Solids,* 54 (7) (2006) 1479-1492.

[8] M. Doyoyo and J. W. Hu, Multi-axial failure of metallic strut-lattice materials composed of short and slender struts, *International Journal of Solids and Structure*. 43 (2006) 6115-6139.

[9] D. Lim, H. S. Kim, Y. H. Kim, Y. H. Kim and S. T. S. Al-Hassani, Stress analysis of two-dimensional cellular materials with thick cell struts, *Journal of Mechanical Science and Technology,* 22 (2008) 835-845.

[10] S. M. Lake, Stiffness and strength tailoring in uniform space-filling truss structures, NASA TP-3210, (1992).

[11] J. Aboudi and R. Gilat, Micromechanical analysis of lattice blocks. *International Journal of Solids and Structure*, 42 (2005) 4372-4392.

[12] S. Gonella and M. Ruzzene, Homogenization and equivalent in-plane properties of two-dimensional periodic lattice. *International Journal of Solids and Structure*, 45 (2008) 2897-2915.

[13] D. Mohr, Multi-scale finite-strain plasticity model for stable metallic honeycombs incorporating micro-structural evolution, *International journal of plasticity*, 22 (2006) 1899-1923.

[14] J. C. Wallach and L. J. Gibson, Mechanical behavior of a three-dimensional truss material. *International Journal of Solids and Structure*, 38 (2001) 7181-7196.

[15] E. Ziegler, M. Accorsi and M. Bennett, Continuum plate model for lattice block material, *Mechanics of Materials*, 36 (2004) 753-766.

[16] P. Suquet, Elements of homogenization for inelastic solid mechanics. In: E. Sanchez-Palencia, A. Zaoui (Eds.), Homogenization techniques for composite media, *Lecture notes in physics,* Springer-Verlag, Berlin, (1987) 193-278.

[17] A. H. Nayfeh and M. S. Hefzy, Continuum modeling of three-dimensional truss-like space structures, *AIAA Journal,* (1978) 16 (8) 779-787.

[18] T. Zhang and J. Lee, A plasticity model for cellular materials with open-celled structure, *International Journal of Plasticity,* (2003) 19 749-770.

[19] R. S. Kumar and D. L. McDowell, Generalized continuum modeling of 2-D periodic cellular solids. *International Journal of Solids and Structure,* (2004) 41 7399-7422.

[20] S. Gonella and M. Ruzzene, Homogenization and equivalent in-plane properties of two-dimensional periodic lattice, *International Journal of Solids and Structure,* (2008) 45 2897-2915.

[21] M. A. Crisfield, Non-linear finite element analysis of solids and structures, *John Wiley & Sons*, London, vol. I (1997) 152-200.

[22] ABAQUS, v. 6.7-1, Theory and User's Manual, Hibbit, Karlsson & Sorensen, Inc., Pawtucket, RI., (2006).

[23] N. Wicks and J. W. Hutchinson, Optimal truss plates. *International Journal of Solids and Structure,* (2001) 38, 5165-5183.

Dr. Taehyo Park received a B.S. degree in Civil Engineering from Hanyang University. He then went to receive his M.S. and Ph.D. degree from University of Iowa and Louisiana State University, USA, respectively. He has been a professor at Department of Civil Engineering in Hanyang University since 2000. His major area of study is the mechanics of composites, continuum damage mechanics, computational solid mechanics, and finite element analysis.

Dr. Won-Sup Hwang received a B.S. and M.S. degree in Civil Engineering from Inha University. He then went to receive his Ph.D. degree from Osaka University in Osaka, Japan. He has been a professor at Department of Civil Engineering in Inha University since 1995. His major area of study is hybrid structure design, structural analysis, and composite materials.

Dr. Jong Wan Hu received his MS degrees from (1) G.W.W. School of Mechanical Engineering and (2) School of Civil and Environmental Engineering, respectively, in Georgia Institute of Technology. He then received his Ph.D. degree from School of Civil and Environmental Engineering, Georgia Institute of Technology. Dr. Hu was a Post-Doctorate Research Fellow at Structural, Mechanics, and Material Research Group in Georgia Institute of Technology. Currently, he has been a BK21 research assistant professor at Department of Civil Engineering in Hanyang University. He has been active in the member of ASME and ASCE. He research interests are in the area of computational solid mechanics, composite materials, and plasticity modeling.